Refined determination of the weak mixing angle at low energy

M. Atzori Corona,[1,2,*] M. Cadeddu,[2,†] N. Cargioli,[1,2,‡] F. Dordei,[2,§] and C. Giunti[3,‖]

[1]*Dipartimento di Fisica, Università degli Studi di Cagliari, Complesso Universitario di Monserrato—S.P. per Sestu Km 0.700, 09042 Monserrato (Cagliari), Italy*

[2]*Istituto Nazionale di Fisica Nucleare (INFN), Sezione di Cagliari, Complesso Universitario di Monserrato—S.P. per Sestu Km 0.700, 09042 Monserrato (Cagliari), Italy*

[3]*Istituto Nazionale di Fisica Nucleare (INFN), Sezione di Torino, Via P. Giuria 1, I–10125 Torino, Italy*

(Received 24 May 2024; accepted 23 July 2024; published 19 August 2024)

The weak mixing angle is a fundamental parameter of the electroweak theory of the standard model whose measurement in the low-energy regime is still not precisely determined. Different probes are sensitive to its value, including atomic parity violation, coherent elastic neutrino-nucleus scattering, and parity-violating electron scattering on different nuclei. In this work, we attempt for the first time to combine all these various determinations by performing a global fit that also takes into account the unavoidable dependence on the experimentally poorly known neutron distribution radius of the nuclei employed, for which a new measurement using proton-cesium elastic scattering became available. By using all present direct determinations of the neutron distribution radius of cesium, we find $\sin^2\vartheta_W = 0.2396^{+0.0020}_{-0.0019}$, which should supersede the previous value determined from atomic parity violation on cesium. When including electroweak only, but also indirect, determinations of the neutron distribution radius of cesium, the uncertainty reduces to 0.0017, maintaining the same central value and showing excellent agreement independently of the method used.

DOI: 10.1103/PhysRevD.110.033005

I. INTRODUCTION

The standard model (SM) of the electroweak interactions is described by the gauge group $\mathrm{SU}(2)\times\mathrm{U}(1)$, with the $i = 1, 2, 3$ gauge bosons W^i_μ and B_μ for the SU(2) and U(1) groups, respectively, and the corresponding gauge coupling constants g and g'. After spontaneous symmetry breaking, the physical Z boson and photon mediators are obtained from a rotation of the basis of the two gauge bosons, B_μ and W^3_μ. The angle of this rotation is known as the weak mixing angle, $\vartheta_\mathrm{W} \equiv \tan^{-1}(g'/g)$, also referred to as the Weinberg angle [1]. In practice, the quantity $\sin^2\vartheta_\mathrm{W}$ is usually quoted instead of the weak mixing angle itself.

The experimental determination of $\sin^2\vartheta_\mathrm{W}$ and its dependence on the energy scale of the process, so-called running, provides a direct probe of physics phenomena beyond the SM (BSM). Its value is extracted from neutral-current processes and Z-pole observables. More in detail, at the Large Electron-Positron (LEP) Collider [2], it was possible to achieve the most precise measurements of $\sin^2\vartheta_\mathrm{W}$ in the high-energy electroweak (EW) sector, in perfect agreement with other collider determinations [1] (Tevatron, LHC, and SLC). In the midenergy range, the most precise result has been derived from the measurement of the weak charge of the proton, Q^p_W, performed by the Q_weak Collaboration and found to be $Q^p_W = 0.0719 \pm 0.0045$ [3], showing excellent agreement with the predicted SM running. Moving to the low-energy sector [4], the most precise weak mixing angle measurement so far belongs to the so-called atomic parity violation (APV) experiments, also known as parity nonconservation (PNC), using cesium atoms [5,6], namely, $\sin^2\vartheta_W = 0.2367 \pm 0.0018$. This value is slightly smaller than the SM prediction at near zero momentum transfer, $\mathrm{Q} = 0$, calculated in the so-called modified minimal subtraction ($\overline{\mathrm{MS}}$) renormalization scheme, $\sin^2\vartheta^{\mathrm{SM}}_W(\mathrm{Q}=0) = 0.23863 \pm 0.00005$ [1,7,8]. Atomic parity violation is caused by the weak interaction, and it is manifested in P-violating atomic observables [9]. Other targets have also been used, even if with less precise outcomes, and of interest for this work is the measurement of APV in lead [10,11]. Such experiments play a unique role complementary to those at high energy [12]. In particular, APV is highly sensitive to extra light Z' bosons

*Contact author: mattia.atzori.corona@ca.infn.it
†Contact author: matteo.cadeddu@ca.infn.it
‡Contact author: nicola.cargioli@ca.infn.it
§Contact author: francesca.dordei@cern.ch
‖Contact author: carlo.giunti@to.infn.it

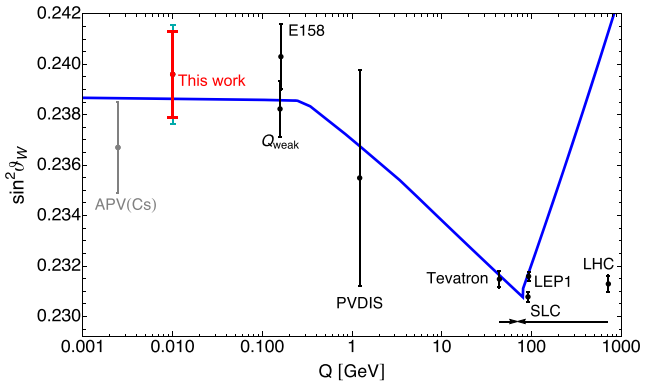

FIG. 1. Variation of $\sin^2\vartheta_W$ with scale Q. The SM prediction is shown as the solid curve, together with experimental determinations in black at the Z-pole [1] (Tevatron, LEP1, SLC, LHC), from APV on cesium [5,6] [APV(Cs)], Møller scattering [14] (E158), deep inelastic scattering of polarized electrons on deuterons [15] (PVDIS), and the result from the proton's weak charge [3] ($Q_{\rm weak}$). For illustration purposes, the Tevatron and LHC points have been shifted horizontally to the left and right, respectively. In cyan is the result derived in this paper when combining APV(Cs) with CEνNS COHERENT CsI data [16,17] and the neutron skin determination at the CSRe facility [18]. A similar result, slightly more precise, is obtained considering electroweak probes only and is shown in red.

predicted by BSM theories, underscoring the need for improved experimental determinations of $\sin^2\vartheta_W$ in the low-energy regime [12,13].

A summary of the most precise weak mixing angle measurements as a function of the scale, Q, is shown in Fig. 1, along with the SM predicted running of $\sin^2\vartheta_W$, calculated in the $\overline{\rm MS}$ renormalization scheme [1,7,8].

In the low-energy sector, there are two other electroweak probes that are mildly sensitive to the weak mixing angle. They are the coherent elastic neutrino-nucleus scattering (CEνNS) [19] and measurements of parity violation in electron scattering (PVES) on nuclei. The first process has been observed so far in three targets, namely, in cesium iodide (CsI) [16,17], in argon (Ar) [20], and very recently in germanium (Ge) [21] by the COHERENT Collaboration using a spallation neutron source. Moreover, a strong preference for CEνNS was reported in Ref. [22] using antineutrinos from the Dresden-II reactor and a germanium target, even though this observation is in mild tension with recent CONUS data [23] and relies on an enhancement at low-energy of the ionization yield [24], whose origin remains still unexplained [25]. The CEνNS cross section depends on the value of $\sin^2\vartheta_W$ through the neutral-current vector coupling of the proton g_V^p [19,26,27], whose tree-level value is given by $g_V^p = \frac{1}{2} - 2\sin^2\vartheta_W^{\rm SM}(Q=0) \simeq 0.0227$. More precise values are determined by taking into account the radiative corrections in the $\overline{\rm MS}$ scheme, following Refs. [1,26]. Being the proton contribution subdominant with respect to the neutron one, only broad constraints on $\sin^2\vartheta_W$ can be obtained [27–33]. The most recent updated result is $\sin^2\vartheta_W = 0.231^{+0.027}_{-0.024}$ [27], obtained from the latest COHERENT CsI data [17].

PVES consists of polarized electron-nucleus scattering, e.g., in lead, that happens through both the weak and the electromagnetic currents. Isolating the first contribution, it provides an interesting way to assess the nuclear structure, but it can also be used to put constraints on $\sin^2\vartheta_W$. This has been recently suggested in Ref. [34], using the latest PVES measurements on lead released by the PREX-II Collaboration [35].

Historically, the APV measurement in cesium has moved significantly over the years (see the inset of Fig. 9 of Ref. [27]), being mostly lower than the SM prediction, motivating further investigation of all the inputs entering this measurement. Moreover, the extraction of the weak mixing angle value using electroweak probes (APV, CEνNS, and PVES) is always affected by the limited knowledge of the so-called neutron skin of the nuclei used as a target [36]. The latter is defined as $\Delta R_{\rm np} \equiv R_{\rm n} - R_{\rm p}$ and quantifies the difference between the neutron and the proton root-mean-square nuclear distribution radii, $R_{\rm n}$ and $R_{\rm p}$, respectively, where the latter is experimentally well-known from electromagnetic measurements [37]. The usage of an extrapolated or imprecise value of the neutron radius of cesium or lead would bias the extraction of $\sin^2\vartheta_W$ and vice versa, misinterpreting potential signs of BSM physics. It is thus of pivotal importance to exploit all available inputs on $\Delta R_{\rm np}$ and $\sin^2\vartheta_W$ in a combined measurement, in order to take advantage of possible correlations and minimize external assumptions.

The difficulty in measuring $\Delta R_{\rm np}$ is that the nuclear neutron distribution can be probed only by exploiting the strong or weak forces. The effects of the weak neutral-current interactions, embodied by the weak charge of the nucleus, are known with good approximation, thus making these measurements systematically clean. However, the statistical uncertainty is still quite limited. On the contrary, the results of experiments with hadron probes are more precise but their interpretation is difficult since the effects of strong-force interactions cannot be calculated with sufficient approximation and the interpretation can be done only by assuming a strong-interaction model with all its limitations [36]. On top of that, the cesium neutron radius determination with hadronic probes has been historically experimentally challenging due to the low melting point and spontaneous ignition in air, resulting up to now for the APV $\sin^2\vartheta_W$ determination in the utilization of an extrapolated $R_{\rm n}({\rm Cs})$ value from antiprotonic atom x-ray data [38]. However, recently, a new direct measurement of the cesium neutron skin, 0.12 ± 0.21 fm, appeared [18], obtained using proton-cesium elastic scattering at low momentum transfer and an in-ring reaction technique at the Cooler Storage Ring (CSRe) at the Heavy Ion Research Facility in Lanzhou, which can be included in the derivation of

$\sin^2\vartheta_W$. The authors employed this value to re-extract the COHERENT $\sin^2\vartheta_W$ value by fitting the CEνNS CsI dataset, finding $\sin^2\vartheta_W = 0.227 \pm 0.028$.

Taking into account all these recent developments, in this work, we combine all the available measurements of $R_n(\mathrm{Cs})$, $R_n(\mathrm{Pb})$, and $\sin^2\vartheta_W$ in a global fit to extract the most up to date and precise determination of the weak mixing angle at low energy. Moreover, to better check the consistency among the different inputs and techniques, we also compare the electroweak-only determination with the averages obtained using strong probes.

II. RESULTS

To start with, we combine all available measurements using cesium atoms, namely, atomic parity violation on cesium, APV(Cs), CEνNS on CsI, referred to as COH, and the recent determination of $R_n(\mathrm{Cs})$ at the CSRe facility. The APV observable is the weak charge of the nucleus $Q_W(\mathrm{Cs})$, which is extracted by means of the experimental determination of the ratio of the parity-violating amplitude, E_{PNC}, and the Stark vector transition polarizability, β, and by calculating theoretically E_{PNC} in terms of Q_W. For the latter, the Particle Data Group (PDG) uses the theoretical prediction of the PNC amplitude $(\mathrm{Im}\,E_{\mathrm{PNC}})^{\mathrm{wns}}_{\mathrm{th}} = (0.8995 \pm 0.0040) \times 10^{-11}|e|a_B\frac{Q_W}{N}$ of Ref. [6], referred to hereafter as APV PDG, where Im stands for the imaginary part, a_B is the Bohr radius, N is the number of neutrons in the nucleus, and $|e|$ is the absolute value of the electric charge. The apex w.n.s. means that the neutron skin correction has not already been implemented, given that we want to extract this correction from the combined fit using external inputs. In this work, for the PNC amplitude, we use the more precise value recently calculated in Ref. [39], referred to as APV 21, which exploits a variant of the perturbed relativistic coupled-cluster theory which treats the contributions of the core, valence, and excited states to the spin-independent parity-violating electric dipole transition amplitude on the same footing, unlike the previous high precision calculations. This latter result is in slight tension with that used by the PDG and equal to $(\mathrm{Im}\,E_{\mathrm{PNC}})^{\mathrm{wns}}_{\mathrm{th}} = (0.8931 \pm 0.0027) \times 10^{-11}|e|a_B\frac{Q_W}{N}$. Besides being more precise, it is also in better agreement with those reported in Refs. [40,41]. For completeness, in Appendix B, we repeat all the results reported in this work using APV PDG.

To combine APV(Cs) and COHERENT CsI, we follow the technique initially developed in Ref. [42] and the latest prescriptions detailed in Ref. [27], adding a prior on $R_n(\mathrm{Cs}) = 4.94 \pm 0.21$ fm[1] coming from CSRe. The only mild assumptions behind this combination are that $\sin^2\vartheta_W$ is constant between the corresponding experimental momentum transfers, $2.4 \lesssim Q \lesssim 100$ MeV, which is true in the absence of BSM effects, and that the ^{133}Cs and ^{127}I neutron skins are the same in order to isolate the contribution of $R_n(\mathrm{Cs})$ when analyzing the COHERENT data. Given the fact that the neutron skin difference for these two nuclei is expected to be small compared to the current precision of experimental data, this choice is a fair approximation. We also checked that the fitting for an average value of the rms neutron radii of ^{133}Cs and ^{127}I gives the same output. The result is shown in Fig. 2 at different confidence levels (CLs), while the numerical values can be found in Table I.

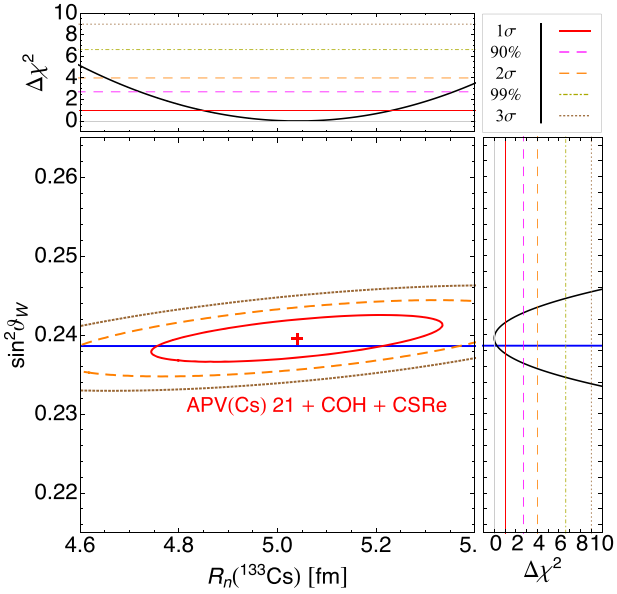

FIG. 2. Constraints on the weak mixing angle $\sin^2\vartheta_W$ and the Cs neutron radius $R_n(^{133}\mathrm{Cs})$ obtained from a combined APV(Cs) $21 + \mathrm{COH} + \mathrm{CSRe}$ fit at different CLs $(1-2-3\sigma)$, together with their marginalizations in the side panels. The blue line indicates the theoretical low-energy value of the weak mixing angle, $\sin^2\vartheta_W^{\mathrm{SM}}(\mathrm{Q}=0)$.

This determination of $\sin^2\vartheta_W$ depends on the CSRe determination of $R_n(\mathrm{Cs})$, which dominates the COHERENT and APV(Cs) sensitivity on the neutron distribution radius. In order to check the impact of relying so heavily on a measurement of the neutron distribution radius obtained using strong probes, we perform a further determination of $\sin^2\vartheta_W$ using electroweak probes only. To do so, we exploit two additional EW probes, namely, PREX-II and APV, on lead. The former determines the weak form factor value at the experimental mean momentum transfer, $Q_{\mathrm{PREX\text{-}II}} \simeq 78$ MeV [35], which depends on both the neutron distribution radius of lead and $\sin^2\vartheta_W$. A simultaneous fit of these two parameters can be achieved following the method developed in Ref. [34] and produces an almost fully degenerate oblique band in the

[1]The latter radius has been obtained starting from the skin measured in Ref. [18] and using the rms proton radius of cesium $R_p(\mathrm{Cs}) = 4.821(5)$ fm [27,37,43] and the neutron radius $\langle r_n^2\rangle \simeq \langle r_p^2\rangle = 0.708$ fm^2 [44].

TABLE I. Summary of the constraints at 1σ CL obtained in this work on the weak mixing angle $\sin^2\vartheta_W$ and on the Cs neutron radius $R_n(^{133}\mathrm{Cs})$. The different labels refer to the COHERENT CsI data (COH), APV (Cs) data using the PNC amplitude of Ref. [39], and the CSRe determination of $R_n(^{133}\mathrm{Cs})$. The electroweak result (EW combined) combines APV(Cs)+COH with PREX-II and APV determinations on lead. The global fit includes all of the above plus the non-EW determinations of R_n on lead.

	$\sin^2\vartheta_W$	$R_n(^{133}\mathrm{Cs})$(fm)
APV(Cs) + COH + CSRe	$0.2396^{+0.0020}_{-0.0019}$	5.04 ± 0.19
EW combined	0.2396 ± 0.0017	5.04 ± 0.06
Global fit	0.2387 ± 0.0016	4.952 ± 0.009

R_n(Pb)-$\sin^2\vartheta_W$ plane. To break the degeneracy, the PREX-II result can be combined with the APV experiment on ^{208}Pb, which is sensitive to the nuclear weak charge at a momentum transfer of $Q_{\mathrm{APV(Pb)}} \sim 8$ MeV. In this case, we assume $\sin^2\vartheta_W$ to be constant between the corresponding experimental momentum transfers, $8 \lesssim Q \lesssim 78$ MeV. Furthermore, a practically model-independent extrapolation can be performed, following the method developed in Ref. [13] and briefly summarized in Appendix A, to translate the R_n(Pb) determination into a measurement of R_n(Cs). In this way, the green contour shown in Fig. 3 is obtained at the 1σ CL. In the same figure, it is possible to judge the good agreement between the different EW probes currently available, namely, APV(Cs), APV(Pb) + PREX-II, and COHERENT CsI. All these probes can be combined together to get a fully EW determination of $\sin^2\vartheta_W$ and R_n(Cs), as shown by the red contour at 1σ in Fig. 3.

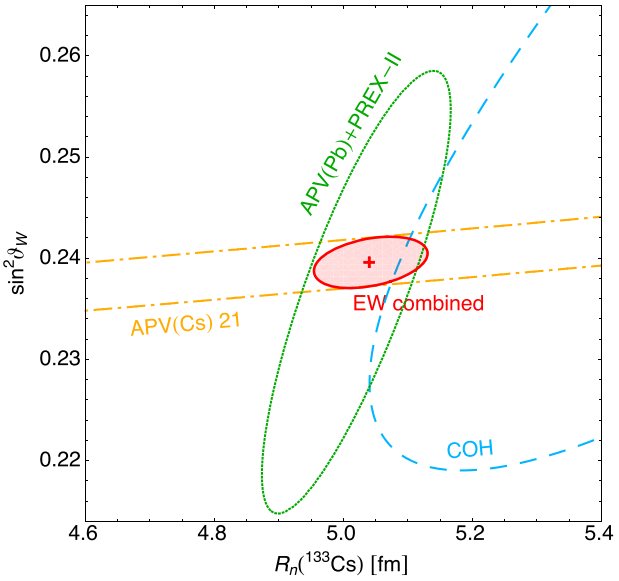

FIG. 3. Individual and combined contours at 1σ CL of the available electroweak probes. Namely, APV(Cs) (orange dash-dotted line), APV(Pb) + PREX-II already converted into R_n(Cs) (dotted green line), and COH CsI (light-blue dashed line). The red solid contour is the combination of all these EW probes, with the red cross indicating the best-fit values.

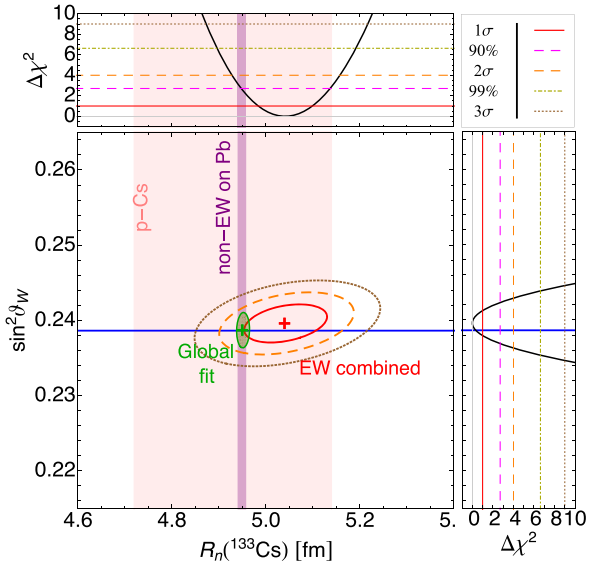

FIG. 4. Combined EW fit at different CLs ($1-2-3\sigma$) and its marginalized $\Delta\chi^2$'s curves in the side panels considering APV(Cs) 21. The pink and purple bands indicate non-EW measurements of the cesium radius, coming from proton scattering on cesium (CSRe) and from the average of non-EW measurements on lead converted into R_n(Cs) using the method explained in Appendix A. In green, the result of the combined APV(Cs)21 + COH + CSRe + PREX-II + APV(Pb) + non-EW(on Pb) fit is shown at 1σ CL. The blue line shows the SM value of the weak mixing angle, $\sin^2\vartheta_W^{\mathrm{SM}}(Q=0)$.

The EW combination is also shown at different CLs and together with the marginalized $\Delta\chi^2$'s curves in Fig. 4. Here, we also compare the EW fit to other non-EW measurements of R_n(Cs), namely, the direct one derived at CSRe using proton-cesium scattering [18] and a more precise determination that is obtained from a conversion of the non-EW measurements of R_n(Pb). The latter average is retrieved by considering all non-electroweak R_n(Pb) determinations in Table 4 of Ref. [45], Table I of Ref. [46], and a recent measurement performed at the LHC [47]. A summary of all the measurements considered is shown in Fig. 5, where it is possible to see that a rather good agreement among all the different techniques is obtained. The average is $\Delta R_{\mathrm{np}}^{\mathrm{non-EW}}(\mathrm{Pb}) = 0.16 \pm 0.01$ fm. For comparison, in the same figure, we also show the EW determination coming from our combined fit of APV(Pb) + PREX-II, namely, $\Delta R_{\mathrm{np}}^{\mathrm{EW}}(\mathrm{Pb}) = 0.262 \pm 0.136$ fm, which also underlines the rather good agreement that can be obtained between EW and non-EW probes as long as in the former the dependence on $\sin^2\vartheta_W$ is taken into account. In addition, all these experimental values are in rather good agreement with the theoretical expected range

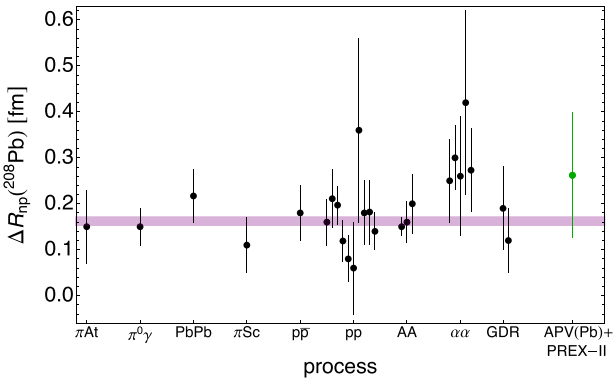

FIG. 5. Summary of available measurements of the lead neutron skin considering different processes [34,52–54]. The black data points indicate non-EW probes, while in green we report the combined APV(Pb) + PREX-II EW measurement. The purple band indicates the 1σ CL value obtained by averaging over all the available non-EW measurements.

$0.13 < \Delta R_{\rm np}(\mathrm{Pb}) < 0.19$ [fm] [48–50] and the first *ab initio* estimate $0.14 < \Delta R_{\rm np}(\mathrm{Pb}) < 0.20$ [fm] [51].

Interestingly, there is extraordinary agreement among the central values obtained for $\sin^2\vartheta_{\rm W}$ when using the strong probe determination at CSRe of $R_{\rm n}(\mathrm{Cs})$ [APV(Cs) + COH + CSRe] and that obtained using exclusively EW probes, as is visible in Table I, with the latter being slightly more precise. This achievement gives confidence that an overall excellent agreement is emerging among EW and strong probe determinations of $R_{\rm n}$, such that the $\sin^2\vartheta_{\rm W}$ result obtained is not too sensitive to the particular dataset or method used. These two determinations, which overlap besides the uncertainty, have also been added to Fig. 1 and should be compared with the previous PDG determination of APV(Cs) [1], with the shift being largely due to the different PNC amplitude used. We would like to underline that our two determinations have uncertainties that are comparable with that of the PDG one.

For completeness, we checked what happens if a global fit of all the measurements shown in Fig. 4 is performed and it is indicated by the green contour in the same figure. Numerical values are also listed in Table I. Clearly, the central value of $\sin^2\vartheta_{\rm W}$ is dominated by the non-EW determinations of $R_{\rm n}(\mathrm{Pb})$, but it is possible to see that there is not much gain on the uncertainty, with the latter being dominated by the uncertainty of APV(Cs). Thus, there is no clear advantage of performing such an aggressive global fit.

III. CONCLUSIONS

Motivated by the lack of a precise determination of the weak mixing angle at low energies, we thoroughly investigate how to exploit correlations among the different probes available in order to maximize the reliability and significance of the $\sin^2\vartheta_{\rm W}$ value that is extracted. In particular, we combine atomic parity violation experiments on cesium and lead nuclei, coherent elastic neutrino-nucleus scattering on cesium iodide, and parity-violating electron scattering on lead by performing a fit that also takes into account the unavoidable dependence on the experimentally poorly known neutron distribution radius of the nuclei employed. For the latter, we also exploit a recent measurement of the cesium neutron distribution radius, obtained using proton-cesium elastic scattering at the CSRe facility. To check the consistency of the results obtained, we compare the weak-mixing angle values obtained using electroweak-only determinations of the neutron distribution radius on cesium and lead nuclei (EW combined) with that obtained using cesium-only determinations of $R_{\rm n}(\mathrm{Cs})$ including also strong probes (APV(Cs) + COH + CSRe). Respectively, we find

$$\sin^2\vartheta_W = \begin{cases} 0.2396 \pm 0.0017(\text{EW combined}) \\ 0.2396^{+0.0020}_{-0.0019}(\text{APV(Cs)} + \text{COH} + \text{CSRe}) \end{cases},$$

where an excellent agreement is visible, with the first method giving a slightly more precise result. These findings underscore the fact that an overall consistent picture is emerging between the values extracted using EW and strong probes, as long as the correlation with the neutron skin is properly taken into account. Finally, given that the latter combination of APV(Cs), COHERENT CsI, and $R_{\rm n}(\mathrm{Cs})$ from CSRe uses direct determinations of $R_{\rm n}(\mathrm{Cs})$, it should supersede the $\sin^2\vartheta_{\rm W}$ value obtained by exploiting APV(Cs)-only with an indirect extrapolation of $R_{\rm n}(\mathrm{Cs})$ [1].

ACKNOWLEDGMENTS

The work of C. G. is supported by the PRIN 2022 research grant "Addressing systematic uncertainties in searches for dark matter," No. 2022F2843L, funded by MIUR.

APPENDIX A: NUCLEAR MODEL PREDICTIONS FOR $\Delta R_{\rm np}(\mathrm{Pb}/\mathrm{Cs})$

In Fig. 6, we show the values of the point neutron skins[2] of ^{208}Pb and ^{133}Cs obtained with various nonrelativistic Skyrme-Hartree-Fock (SHF) [55–60] and relativistic mean field (RMF) [61–70] nuclear models. A clear model-independent linear correlation [29,48,68,71–73] is present between the two neutron skins within the nonrelativistic and relativistic models with different interactions, with a Pearson's correlation coefficient of $\rho \simeq 0.999$. Namely, we find $\Delta R_{\rm np}^{\rm point}(\mathrm{Cs}) = 0.707 \times \Delta R_{\rm np}(\mathrm{Pb}) + 0.016$ fm that can

[2]The physical proton and neutron radii $R_{\rm p,n}$ can be retrieved from the corresponding point radii $R_{\rm p,n}^{\rm point}$ adding in quadrature the contribution of the rms nucleon N radius $\langle r_{\rm N}^2\rangle^{1/2} \simeq 0.84$ fm, that is considered to be approximately equal for the proton and the neutron. Namely, $R_{\rm p,n}^2 = (R_{\rm p,n}^{\rm point})^2 + \langle r_{\rm N}^2\rangle$.

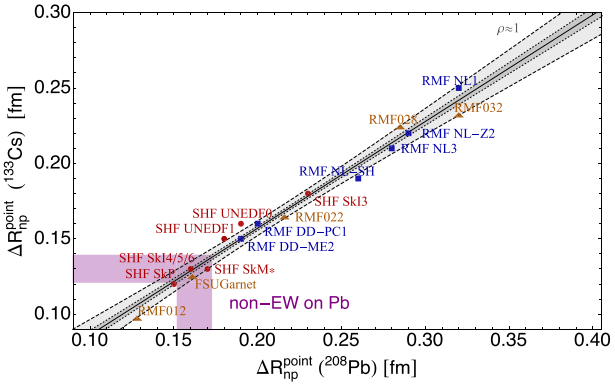

FIG. 6. Correlation between the nuclear model prediction of the lead and cesium neutron skin. The purple-shaded region corresponds to the mean of the neutron skin measured through non-EW probes on lead and its translation into cesium.

be translated into a physical $\Delta R_{\rm np}(\rm Cs)$ determination. We exploit this powerful linear correlation to translate the PREX-II and APV(Pb) combined measurement of the lead neutron skin into a cesium one. Moreover, we also use it to translate the mean of the neutron skin measured through non-EW probes on lead into a determination of the cesium one. The latter is shown by the purple extrapolation in Fig. 6.

APPENDIX B: RESULTS WITH IM $E_{\rm PNC}$ PDG

In this appendix, we report the results using for the atomic parity violation determination in cesium the PNC amplitude $E_{\rm PNC}$ from Ref. [6], referred to as APV(Cs) PDG. The combination of APV(Cs) PDG and COHERENT CsI adding a prior on $R_{\rm n}(\rm Cs) = 4.94 \pm 0.21$ fm coming from CSRe is shown in Fig. 7 at different CLs, while the numerical values can be found in Table II.

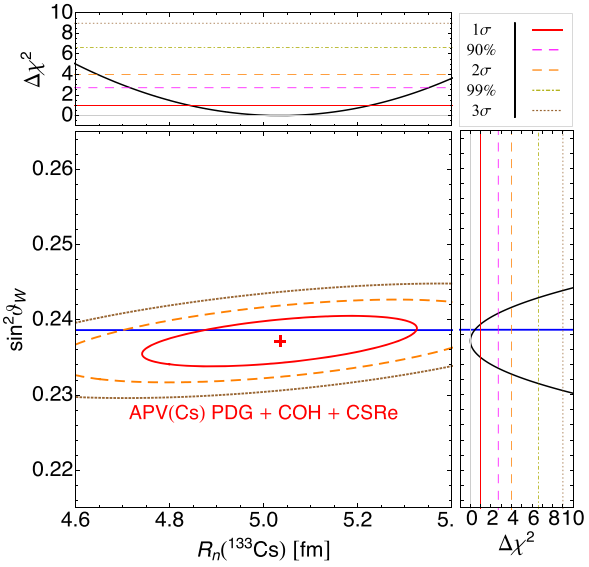

FIG. 7. Constraints on the weak mixing angle $\sin^2\vartheta_{\rm W}$ and the Cs neutron radius $R_{\rm n}(^{133}\rm Cs)$ obtained from a combined APV (Cs) PDG + COH + CSRe fit at different CLs $(1-2-3\sigma)$, together with their marginalizations in the side panels. The blue line indicates the theoretical low-energy value of the weak mixing angle, $\sin^2\vartheta_W^{\rm SM}(\rm Q=0)$.

TABLE II. Summary of the constraints at 1σ CL obtained in this work on the weak mixing angle $\sin^2\vartheta_{\rm W}$ and on the Cs neutron radius $R_{\rm n}(^{133}\rm Cs)$. The different labels refer to the COHERENT CsI data (COH), APV (Cs) PDG data using the PNC amplitude of Ref. [6], and the CSRe determination of $R_{\rm n}(^{133}\rm Cs)$. The electroweak result (EW combined) combines APV(Cs) + COH with PREX-II and APV determinations on lead. The global fit includes all of the above plus the non-EW determinations of $R_{\rm n}$ on lead.

	$\sin^2\vartheta_W$	$R_{\rm n}(^{133}\rm Cs)$(fm)
APV(Cs) + COH + CSRe	0.2372 ± 0.0022	5.04 ± 0.19
EW combined	0.2372 ± 0.002	5.03 ± 0.06
Global fit	$0.2363^{+0.0018}_{-0.0019}$	4.951 ± 0.009

All the EW probes currenlty available, namely, APV(Cs) PDG, APV(Pb) + PREX-II, and COHERENT CsI, are combined to get a fully EW determination of $\sin^2\vartheta_{\rm W}$ and $R_{\rm n}(\rm Cs)$, as shown at different CLs and together with the marginalized $\Delta\chi^2$ curves in Fig. 8. Here, we also compare the EW fit to other non-EW measurements of $R_{\rm n}(\rm Cs)$, namely, the direct one derived at CSRe using proton-cesium scattering [18] and a more precise determination

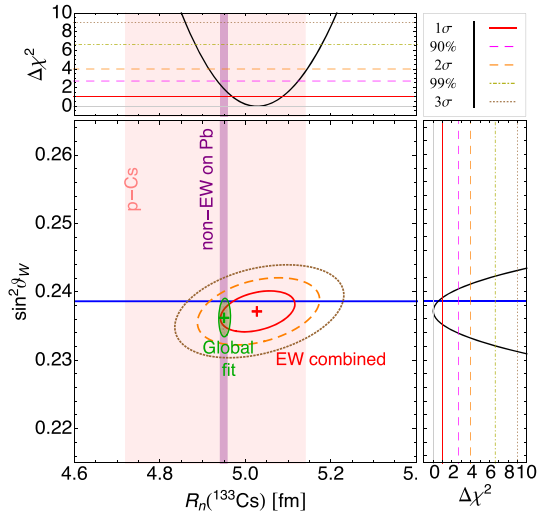

FIG. 8. Combined EW fit at different CLs $(1-2-3\sigma)$ and its marginalized $\Delta\chi^2$ curves in the side panels considering APV(Cs) PDG. The pink and purple bands indicate non-EW measurements of the cesium radius, coming from proton scattering on cesium (CSRe), and from the average of non-EW measurements on lead converted into $\rm R_n(Cs)$ using the method explained in Appendix A. In green the result of the combined APV(Cs) PDG+ COH + CSRe + PREX-II + APV(Pb) + non-EW(on Pb) fit is shown at 1σ CL. The blue line shows the SM value of the weak mixing angle, $\sin^2\vartheta_W^{\rm SM}(\rm Q=0)$.

that is obtained from a conversion of the non-EW measurements of $R_n(\mathrm{Pb})$, as explained in Appendix A. For completeness, in Fig. 8, we also show the result of a global fit of all these determinations. It is possible to notice, by comparing Figs. 4 and 8, that using the PNC amplitude E_{PNC} from Ref. [6] [APV(Cs) PDG] results in a $\sin^2\vartheta_W$ value that is slightly smaller than the SM prediction as well as less precise.

[1] R. L. Workman *et al.* (Particle Data Group), Review of particle physics, Prog. Theor. Exp. Phys. **2022**, 083C01 (2022).

[2] S. Schael *et al.* (ALEPH, DELPHI, L3, OPAL, SLD Collaborations, LEP Electroweak Working Group, SLD Electroweak Group, and SLD Heavy Flavour Group), Precision electroweak measurements on the Z resonance, Phys. Rep. **427**, 257 (2006).

[3] D. Androić *et al.* (Qweak Collaboration), Precision measurement of the weak charge of the proton, Nature (London) **557**, 207 (2018).

[4] K. S. Kumar, S. Mantry, W. J. Marciano, and P. A. Souder, Low energy measurements of the weak mixing angle, Annu. Rev. Nucl. Part. Sci. **63**, 237 (2013).

[5] C. S. Wood, S. C. Bennett, D. Cho, B. P. Masterson, J. L. Roberts, C. E. Tanner, and C. E. Wieman, Measurement of parity nonconservation and an anapole moment in cesium, Science **275**, 1759 (1997).

[6] V. A. Dzuba, J. C. Berengut, V. V. Flambaum, and B. Roberts, Revisiting parity non-conservation in cesium, Phys. Rev. Lett. **109**, 203003 (2012).

[7] J. Erler and M. J. Ramsey-Musolf, The weak mixing angle at low energies, Phys. Rev. D **72**, 073003 (2005).

[8] J. Erler and R. Ferro-Hernández, Weak mixing angle in the Thomson limit, J. High Energy Phys. 03 (2018) 196.

[9] B. Roberts, V. Dzuba, and V. Flambaum, Parity and time-reversal violation in atomic systems, Annu. Rev. Nucl. Part. Sci. **65**, 63 (2015).

[10] S. G. Porsev, M. G. Kozlov, M. S. Safronova, and I. I. Tupitsyn, Development of the configuration-interaction + all-order method and application to the parity-nonconserving amplitude and other properties of Pb, Phys. Rev. A **93**, 012501 (2016).

[11] D. M. Meekhof, P. Vetter, P. K. Majumder, S. K. Lamoreaux, and E. N. Fortson, High-precision measurement of parity nonconserving optical rotation in atomic lead, Phys. Rev. Lett. **71**, 3442 (1993).

[12] M. S. Safronova, D. Budker, D. DeMille, D. F. J. Kimball, A. Derevianko, and C. W. Clark, Search for new physics with atoms and molecules, Rev. Mod. Phys. **90**, 025008 (2018).

[13] M. Cadeddu, N. Cargioli, F. Dordei, C. Giunti, and E. Picciau, Muon and electron $g-2$ and proton and cesium weak charges implications on dark Z_d models, Phys. Rev. D **104**, 011701 (2021).

[14] P. L. Anthony *et al.* (SLAC E158 Collaboration), Precision measurement of the weak mixing angle in Moller scattering, Phys. Rev. Lett. **95**, 081601 (2005).

[15] D. Wang *et al.* (PVDIS Collaboration), Measurement of parity violation in electron–quark scattering, Nature (London) **506**, 67 (2014).

[16] D. Akimov *et al.* (COHERENT Collaboration), Observation of coherent elastic neutrino-nucleus scattering, Science **357**, 1123 (2017).

[17] D. Akimov *et al.* (COHERENT Collaboration), Measurement of the coherent elastic neutrino-nucleus scattering cross section on CsI by COHERENT, Phys. Rev. Lett. **129**, 081801 (2022).

[18] Y. Huang *et al.*, Neutron radius determination of ^{133}Cs and constraint on the weak mixing angle, arXiv:2403.03566.

[19] M. Cadeddu, F. Dordei, and C. Giunti, A view of coherent elastic neutrino-nucleus scattering, Europhys. Lett. **143**, 34001 (2023).

[20] D. Akimov *et al.* (COHERENT Collaboration), COHERENT Collaboration data release from the first detection of coherent elastic neutrino-nucleus scattering on argon, arXiv:2006.12659.

[21] S. Adamski *et al.*, First detection of coherent elastic neutrino-nucleus scattering on germanium, arXiv:2406.13806.

[22] J. Colaresi, J. I. Collar, T. W. Hossbach, C. M. Lewis, and K. M. Yocum, Measurement of coherent elastic neutrino-nucleus scattering from reactor antineutrinos, Phys. Rev. Lett. **129**, 211802 (2022).

[23] N. Ackermann *et al.*, Final CONUS results on coherent elastic neutrino nucleus scattering at the Brokdorf reactor, arXiv:2401.07684.

[24] J. I. Collar, A. R. L. Kavner, and C. M. Lewis, Germanium response to sub-keV nuclear recoils: A multipronged experimental characterization, Phys. Rev. D **103**, 122003 (2021).

[25] M. Atzori Corona, M. Cadeddu, N. Cargioli, F. Dordei, and C. Giunti, On the impact of the Migdal effect in reactor CEvNS experiments, Phys. Lett. B **852**, 138627 (2024).

[26] M. Atzori Corona, M. Cadeddu, N. Cargioli, F. Dordei, and C. Giunti, Momentum dependent flavor radiative corrections to the coherent elastic neutrino-nucleus scattering for the neutrino charge-radius determination, J. High Energy Phys. 05 (2024) 271.

[27] M. Atzori Corona, M. Cadeddu, N. Cargioli, F. Dordei, C. Giunti, and G. Masia, Nuclear neutron radius and weak mixing angle measurements from latest COHERENT CsI and atomic parity violation Cs data, Eur. Phys. J. C **83**, 683 (2023).

[28] M. Atzori Corona, M. Cadeddu, N. Cargioli, F. Dordei, C. Giunti, Y. F. Li, C. A. Ternes, and Y. Y. Zhang, Impact of the

Dresden-II and COHERENT neutrino scattering data on neutrino electromagnetic properties and electroweak physics, J. High Energy Phys. 09 (2022) 164.
[29] M. Cadeddu, N. Cargioli, F. Dordei, C. Giunti, Y. F. Li, E. Picciau, C. A. Ternes, and Y. Y. Zhang, New insights into nuclear physics and weak mixing angle using electroweak probes, Phys. Rev. C **104**, 065502 (2021).
[30] M. Cadeddu, F. Dordei, C. Giunti, Y. F. Li, and Y. Y. Zhang, Neutrino, electroweak, and nuclear physics from COHERENT elastic neutrino-nucleus scattering with refined quenching factor, Phys. Rev. D **101**, 033004 (2020).
[31] O. G. Miranda, D. K. Papoulias, G. S. Garcia, O. Sanders, M. Tortola, and J. W. F. Valle, Implications of the first detection of coherent elastic neutrino-nucleus scattering (CEvNS) with Liquid Argon, J. High Energy Phys. 05 (2020) 130.
[32] D. K. Papoulias, T. S. Kosmas, R. Sahu, V. K. B. Kota, and M. Hota, Constraining nuclear physics parameters with current and future COHERENT data, Phys. Lett. B **800**, 135133 (2020).
[33] V. De Romeri, O. G. Miranda, D. K. Papoulias, G. Sanchez Garcia, M. Tortola, and J. W. F. Valle, Physics implications of a combined analysis of COHERENT CsI and LAr data, J. High Energy Phys. 04 (2023) 035.
[34] M. A. Corona, M. Cadeddu, N. Cargioli, P. Finelli, and M. Vorabbi, Incorporating the weak mixing angle dependence to reconcile the neutron skin measurement on Pb208 by PREX-II, Phys. Rev. C **105**, 055503 (2022).
[35] D. Adhikari *et al.* (PREX Collaboration), Accurate determination of the neutron skin thickness of ^{208}Pb through parity-violation in electron scattering, Phys. Rev. Lett. **126**, 172502 (2021).
[36] M. Thiel, C. Sfienti, J. Piekarewicz, C. J. Horowitz, and M. Vanderhaeghen, Neutron skins of atomic nuclei: Per aspera ad astra, J. Phys. G **46**, 093003 (2019).
[37] I. Angeli and K. P. Marinova, Table of experimental nuclear ground state charge radii: An update, At. Data Nucl. Data Tables **99**, 69 (2013).
[38] A. Trzcinska, J. Jastrzebski, P. Lubinski, F. J. Hartmann, R. Schmidt, T. von Egidy, and B. Klos, Neutron density distributions deduced from anti-protonic atoms, Phys. Rev. Lett. **87**, 082501 (2001).
[39] B. K. Sahoo, B. P. Das, and H. Spiesberger, New physics constraints from atomic parity violation in ^{133}Cs, Phys. Rev. D **103**, L111303 (2021).
[40] H. B. Tran Tan, D. Xiao, and A. Derevianko, Parity-mixed coupled-cluster formalism for computing parity-violating amplitudes, Phys. Rev. A **105**, 022803 (2022).
[41] S. G. Porsev, K. Beloy, and A. Derevianko, Precision determination of weak charge of ^{133}Cs from atomic parity violation, Phys. Rev. D **82**, 036008 (2010).
[42] M. Cadeddu and F. Dordei, Reinterpreting the weak mixing angle from atomic parity violation in view of the Cs neutron rms radius measurement from COHERENT, Phys. Rev. D **99**, 033010 (2019).
[43] G. Fricke, C. Bernhardt, K. Heilig, L. A. Schaller, L. Schellenberg, E. B. Shera, and C. W. de Jager, Nuclear ground state charge Radii from electromagnetic interactions, At. Data Nucl. Data Tables **60**, 177 (1995).
[44] M. Cadeddu, F. Dordei, C. Giunti, Y. F. Li, E. Picciau, and Y. Y. Zhang, Physics results from the first COHERENT observation of coherent elastic neutrino-nucleus scattering in argon and their combination with cesium-iodide data, Phys. Rev. D **102**, 015030 (2020).
[45] J. M. Lattimer, Constraints on nuclear symmetry energy parameters, Particles **6**, 30 (2023).
[46] J. T. Zhang, X. L. Tu, P. Sarriguren, K. Yue, Q. Zeng, Z. Y. Sun, M. Wang, Y. H. Zhang, X. H. Zhou, and Y. A. Litvinov, Systematic trends of neutron skin thickness versus relative neutron excess, Phys. Rev. C **104**, 034303 (2021).
[47] G. Giacalone, G. Nijs, and W. van der Schee, Determination of the neutron skin of ^{208}Pb from ultrarelativistic nuclear collisions, Phys. Rev. Lett. **131**, 202302 (2023).
[48] J. Piekarewicz, B. K. Agrawal, G. Colò, W. Nazarewicz, N. Paar, P.-G. Reinhard, X. Roca-Maza, and D. Vretenar, Electric dipole polarizability and the neutron skin, Phys. Rev. C **85**, 041302 (2012).
[49] X. Roca-Maza, X. Viñas, M. Centelles, B. K. Agrawal, G. Colò, N. Paar, J. Piekarewicz, and D. Vretenar, Neutron skin thickness from the measured electric dipole polarizability in ^{68}Ni, ^{120}Sn, and ^{208}Pb, Phys. Rev. C **92**, 064304 (2015).
[50] J. Piekarewicz, Implications of PREX-2 on the electric dipole polarizability of neutron-rich nuclei, Phys. Rev. C **104**, 024329 (2021).
[51] B. Hu *et al.*, *Ab initio* predictions link the neutron skin of ^{208}Pb to nuclear forces, Nat. Phys. **18**, 1196 (2022).
[52] G. Giacalone, G. Nijs, and W. van der Schee, Determination of the neutron skin of ^{208}Pb from ultrarelativistic nuclear collisions, Phys. Rev. Lett. **131**, 202302 (2023).
[53] J. T. Zhang, X. L. Tu, P. Sarriguren, K. Yue, Q. Zeng, Z. Y. Sun, M. Wang, Y. H. Zhang, X. H. Zhou, and Y. A. Litvinov, Systematic trends of neutron skin thickness versus relative neutron excess, Phys. Rev. C **104**, 034303 (2021).
[54] J. M. Lattimer, Constraints on the nuclear symmetry energy from experiments, theory and observations, J. Phys. Conf. Ser. **2536**, 012009 (2023).
[55] J. Dobaczewski, H. Flocard, and J. Treiner, Hartree-Fock-Bogolyubov descriptions of nuclei near the neutrino dripline, Nucl. Phys. **A422**, 103 (1984).
[56] J. Bartel, P. Quentin, M. Brack, C. Guet, and H. B. Hakansson, Towards a better parametrisation of Skyrme-like effective forces: A critical study of the SkM force, Nucl. Phys. **A386**, 79 (1982).
[57] M. Kortelainen, J. McDonnell, W. Nazarewicz, P. G. Reinhard, J. Sarich, N. Schunck, M. V. Stoitsov, and S. M. Wild, Nuclear energy density optimization: Large deformations, Phys. Rev. C **85**, 024304 (2012).
[58] M. Kortelainen, T. Lesinski, J. More, W. Nazarewicz, J. Sarich, N. Schunck, M. V. Stoitsov, and S. Wild, Nuclear energy density optimization, Phys. Rev. C **82**, 024313 (2010).
[59] E. Chabanat, P. Bonche, P. Haensel, J. Meyer, and R. Schaeffer, A Skyrme parametrization from subnuclear to neutron star densities part II. Nuclei far from stabilities, Nucl. Phys. **A635**, 231 (1998).
[60] P. G. Reinhard and H. Flocard, Nuclear effective forces and isotope shifts, Nucl. Phys. **A584**, 467 (1995).
[61] M. M. Sharma, M. A. Nagarajan, and P. Ring, Rho meson coupling in the relativistic mean field theory and description of exotic nuclei, Phys. Lett. B **312**, 377 (1993).

[62] M. Bender, K. Rutz, P. G. Reinhard, J. A. Maruhn, and W. Greiner, Shell structure of superheavy nuclei in selfconsistent mean field models, Phys. Rev. C **60**, 034304 (1999).
[63] G. A. Lalazissis, J. Konig, and P. Ring, A new parametrization for the Lagrangian density of relativistic mean field theory, Phys. Rev. C **55**, 540 (1997).
[64] P. G. Reinhard, M. Rufa, J. Maruhn, W. Greiner, and J. Friedrich, Nuclear ground state properties in a relativistic meson field theory, Z. Phys. A **323**, 13 (1986).
[65] T. Niksic, D. Vretenar, and P. Ring, Relativistic nuclear energy density functionals: Adjusting parameters to binding energies, Phys. Rev. C **78**, 034318 (2008).
[66] T. Niksic, D. Vretenar, P. Finelli, and P. Ring, Relativistic Hartree-Bogolyubov model with density dependent meson nucleon couplings, Phys. Rev. C **66**, 024306 (2002).
[67] J. A. Hernandez, Weak nuclear form factor: Nuclear structure and coherent elastic neutrino-nucleus scattering, Master's thesis, Florida State University, 2019.
[68] J. Yang, J. A. Hernandez, and J. Piekarewicz, Electroweak probes of ground state densities, Phys. Rev. C **100**, 054301 (2019).
[69] W.-C. Chen and J. Piekarewicz, Building relativistic mean field models for finite nuclei and neutron stars, Phys. Rev. C **90**, 044305 (2014).
[70] W.-C. Chen and J. Piekarewicz, Searching for isovector signatures in the neutron-rich oxygen and calcium isotopes, Phys. Lett. B **748**, 284 (2015).
[71] H. Zheng, Z. Zhang, and L.-W. Chen, Form factor effects in the direct detection of isospin-violating dark matter, J. Cosmol. Astropart. Phys. 08 (2014) 011.
[72] T. Sil, M. Centelles, X. Vinas, and J. Piekarewicz, Atomic parity non-conservation, neutron radii, and effective field theories of nuclei, Phys. Rev. C **71**, 045502 (2005).
[73] T.-G. Yue, L.-W. Chen, Z. Zhang, and Y. Zhou, Constraints on the symmetry energy from PREX-II in the multi-messenger era, Phys. Rev. Res. **4**, L022054 (2022).